Research Article

Olga Mareeva*, Vladimir Ermilov, Vera Snezhko, Dmitrii Benin, and Alexander Bakshtanin

Impact of the reinforced metal structure on the mechanical properties foamed aluminium composites at the load

https://doi.org/10.1515/cls-2021-0026
Received Apr 22, 2021; accepted Jul 20, 2021

Abstract: This paper is an experimental study of the quasi-static mechanical compressive properties of the reinforced closed-cell aluminum alloy foams with different cell orientations at different strain rates. The reinforced foam samples were obtained via the powder metallurgical route. The results of the compression tests revealed that the deformation behavior and mechanical properties of foamed aluminum composites are highly dependent on the orientation of the reinforcing mesh. Differences in the deformation behavior of foams appear to be influenced by the mechanical properties of the matrix material, by foam deformation mechanisms, and by the mechanical properties of the reinforcement. The yield stress, plateau stress, densification stress, and energy absorption capacity of unreinforced foam samples improved linearly with increasing strain rate due to dynamic recrystallization and softening of the foam matrix material. The reinforced foam samples exhibit nonlinear deformation behavior. It was also found that the mechanical properties reduction of transverse reinforced foams was slightly lower compared to foams with longitudinal reinforcement at varying strain rates because of the large contribution of the mechanical properties of the reinforcement. The results of the present study can be employed to modelling and obtain impact-resistant fillers for complex structures in transport construction.

Keywords: aluminium foam, densification strain, metal matrix composite, reinforcement, strain rate

1 Introduction

At present, impact resistance plays a vital role in ensuring the structural integrity of metal structures under impact loading, e.g., in a vehicle to protect passengers and reduce the likelihood of damage during vehicle-barrier collisions [1, 2]. Over the past decade, the major challenge facing engineers and researchers has been that of seeking lightweight materials with a high specific strength, an excellent vibration damping capacity, high energy absorption properties, and a high crushing strength performance [3, 4]. These materials include various alloys, metal and polymer composites, and metal foams [5]. The most popular candidates are aluminum foams and tubular structures, which due to their excellent mechanical properties and low weight are appropriate for use in a limitless range of structural and functional applications. Thanks to their excellent properties, including good resistance to corrosion, high sound and vibration damping capabilities, and high energy absorption, aluminum foams are widely used in aerospace, motor vehicle production, aircraft, and shipbuilding [6, 7].

The mechanical properties of aluminum foam rely on structural features, namely the relative density, pore topology (open or closed), cell size, cell shape, and cell distribution [8]. Such porous materials (foams) either are made of pure aluminum or incorporate it as a matrix, which makes them aluminum matrix syntactic foams (AMSFs) or composite aluminum foams (CAFs) [9]. When investigating the microstructure and quasi-static compression properties of AMSFs reinforced with glass cenospheres, it was found that their hardening mechanisms were influenced not only by the cell size, but also by the physical properties of the ma-

***Corresponding Author: Olga Mareeva:** Department of Engineering Structures, Russian State Agrarian University - Moscow Timiryazev Agricultural Academy, Moscow, 127015, Russian Federation, E-mail: olmareeva@rambler.ru
Vladimir Ermilov: Department of Vehicles and Technosphere Safety, Cherepovets State University, Cherepovets, 162600, Russian Federation
Vera Snezhko: Department of Information Technology in APC, Russian State Agrarian University - Moscow Timiryazev Agricultural Academy, Moscow, 127015, Russian Federation
Dmitrii Benin: Department of Information Technology in APC, Russian State Agrarian University - Moscow Timiryazev Agricultural Academy, Moscow, 127015, Russian Federation
Alexander Bakshtanin: Department of Integrated Water Management and Hydraulics, Russian State Agrarian University - Moscow Timiryazev Agricultural Academy, Moscow, 127015, Russian Federation

trix and cenospheres [10]. Another observation was that the values for specific energy absorption and plateau stress of glass cenosphere-reinforced syntactic foams tended to increase with a greater volume fraction of cenospheres, a smaller interface thickness, and a specific alloy. Hence, it appears that besides pore morphology, the impact resistance of composite foams is influenced by the amount of reinforcing agent and its mechanical properties. As for CAFs reinforced with silicon carbide (SiC-15, 30, 45, and 60 wt.%) [11], their values for hardness and transverse rapture strength went up with increase in the volume fraction of SiC. In addition to that, they exhibited better ballistic performance as they absorbed the kinetic energy of the projectile with the lowest penetration depth.

Aluminium alloyed with silicon, $AlSi_{10}Mg$, is one of the most used filler materials for making metal pipes because Si addition improves the flowability of powder and thus helps to avoid exfoliation and hot cracking. At the same time, Mg addition helps to suppress the oxidation of Al matrix during fabrication and reacts with Si to form Mg_2Si phase, which is associated with the age-hardening effect [12, 13]. Another excellent filler that is appropriate for fabricating metal pipes is aluminum *foam* as it helps to increase the impact resistance of tubular structures. Filling metal pipes with foam also improves the crushing force response of the tube [14] and gives the pipe additional strength to withstand oblique loading [15]. Given the above, it is very important to examine and enhance the mechanical properties of aluminum foams.

One way to improve the mechanical properties of an aluminum foam is to internally reinforce it. Some examples of internal reinforcements are ceramic spheres, steel wires, sheets, and grids [16]. AMSFs reinforced with mixed-oxide ceramic hollow spheres have demonstrated excellent compressive elasticity [17], and those reinforced with rectangular pieces of wire mesh wrapped around the precursor had greater strength properties [18, 19]. Some structures are reinforced with net-shape steel sheets [20]. This is done by foaming of a precursor material through the powder metallurgical pathway. The steel netting is infiltrated with molten material and thus forms a bond with the aluminum foam [21, 22]. This reinforcement improves not only the mechanical properties of the aluminum foam, but also its energy absorption capability. However, the position of the reinforcement may affect the result.

Therefore, it is crucial to understand how the mechanical behavior of composite materials changes depending on the orientation and location of a reinforcing object in the matrix to obtain new knowledge and generate new strategies for creating reinforced lightweight composite structures. This study aims to investigate how the orientation of a thin reinforcing steel mesh affects the compression properties of porous metal-matrix composites. For this, porous aluminum alloys reinforced with a stainless steel wire mesh located in different places were tested for impact resistance and energy absorption under quasi-static compression at different strain rates.

2 Materials and methods

2.1 Materials and composite fabrication method

For this study, three kinds of 50 mm × 500 mm × 500 mm aluminum foam specimens were fabricated: a unreinforced specimen, a specimen reinforced with a steel wire mesh in transverse direction (transverse reinforced), and a specimen reinforced with a steel wire mesh in longitudinal direction (longitudinal reinforced). The closed-cell aluminum alloy foams were prepared by powder metallurgical route from $AlSi_{10}Mg$ and stabilized using 10 wt% SiC particles as a thickener and titanium hydride (TiH_2) powder as a foaming agent. Some composites were reinforced with a stainless steel wire mesh embedded either longitudinally or transversely in the precursor, as depicted by Figure 1.

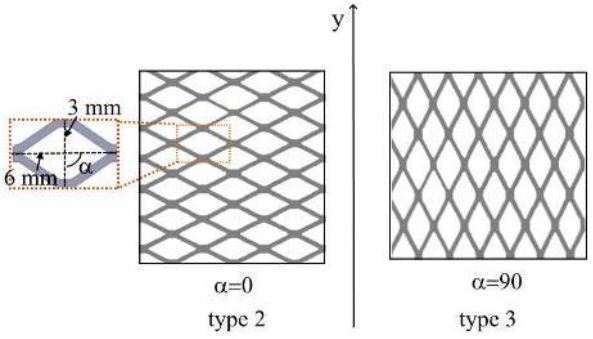

Figure 1: Orientation of reinforcement cells in the aluminum matrix along the y-axis (according to the loading direction). The insert is to show cell dimensions.

The reinforcements with a specific gravity of 3.5 kg/m^2 had a diamond shape (6 mm × 3 mm) and a 0.6 mm × 1 mm wire. The mesh was from EN 1.4301 stainless steel (X5CrNi18-10) [23], containing 0.12% carbon, 18% chromium, 10% nickel, and up to 1% other impurities. The reinforcements were inserted into a specially prepared mold together the precursors. During foam expansion, the mesh sheets were infiltrated with molten material, thus

forming a strong bond (due to the reaction between the liquid foam alloy and the wire mesh). For this, the $AlSi_{10}Mg$ alloy with 10 wt% SiC (size, 20 mm) was placed inside a ceramic crucible and heated at 680 °C in a furnace. The melt was then mechanically stirred for 2 minutes at 850 rpm to ensure proper mixing. Afterwards, 0.8 wt% of TiH_2 was added to the melt for foaming and stirred at about 1000 rpm for 1 minute. Then, a reinforcing mesh was inserted and melt expansion was maintained at 640 °C for 2 minutes. After foaming, all samples were cooled down under air atmosphere [24].

Samples were cut into smaller sheets (geometry 30 mm × 30 mm × 30 mm) using an electric spark cutter. The densities of these samples were measured using the Archimedes method from the mass and volume. The porosity was calculated by the following formula:

$$p = \frac{\rho_0 - \rho_f}{\rho_0} \times 100\% \quad (1)$$

where: p is the porosity, ρ_0 is the density of the parent alloy, ρ_f is the density of the alloy foam.

For analysis, 90 samples with an average density of 440 kg/m^3 were selected. Other samples with a density above or below the accepted mean value by 10% were excluded from further experiments. The porosity value varied in the range between 78% and 83%.

2.2 Quasi-static compression tests

The quasi-static compression tests were performed with an INSTRON FastTrack 8800 test control system. Measurement data were displayed on a computer screen and interpreted using a FastTrack DAX data acquisition software. To assess the energy absorption capability, all samples were subjected to different loads under different strain rates, namely 0.0025, 0.025, and 0.25 s^{-1}. All tests were carried out at room temperature following the ISO13314 standard [25].

To obtain reproducible and reliable results, 10 samples were used for each test conditions. The sample was placed on a special platform and subjected to unidirectional axial loading. Those samples that were reinforced were loaded along the y-axis, as shown in Figure 1. In order to avoid friction between the sample and crosshead, molybdenum disulfide (lubricant) was used.

The mechanical properties of samples were determined from a typical strass-strain curve of a porous metal composite (Figure 2) [26].

The stress-strain curves in point exhibit three distinct regions: the linear elastic region, the yield region, and the densification region. In quasi-static compression tests, the

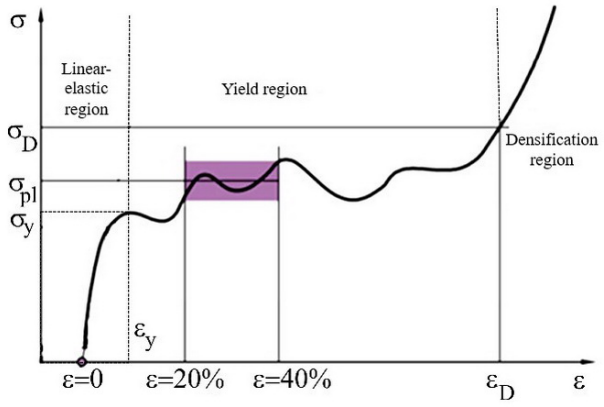

Figure 2: A typical stress-strain curve for determining mechanical properties of porous metal composites in compression tests [26].

following mechanical characteristics were thus determined. The slope of the first region represents a quasi-elastic modulus E_{qe}, which was used to determine the compressive yield stress σ_y and the corresponding strain ε_y. As it can be seen, the compressive yield stress $\sigma_{20\%}$ and $\sigma_{40\%}$ is associated with 20% and 40% compressive strain, respectively. The plateau stress σpl is defined as the arithmetic mean of stresses at $\sigma_{20\%}$ and $\sigma_{40\%}$ compressive strain. The compressive deformation σ_D is a point on the stress-strain curve that equals

$$\sigma_d = 1.3\sigma_{pl} \quad (2)$$

and the related compressive strain is ε_D.

The specific energy absorption W is the amount of energy required to deform a test sample, which can be expressed as follows [26]:

$$W = \int_0^{\varepsilon} \sigma d\varepsilon \quad (3)$$

where: ε is the applied stress and σ is the strain (deformation of the material that results from applied stress).

The specific energy absorption W_D at densification strain is given as follows:

$$W_D = \int_0^{\varepsilon_D} \sigma d\varepsilon \quad (4)$$

3 Results

Figure 3 is a display of stress-strain diagrams for three composite samples under different loading conditions.

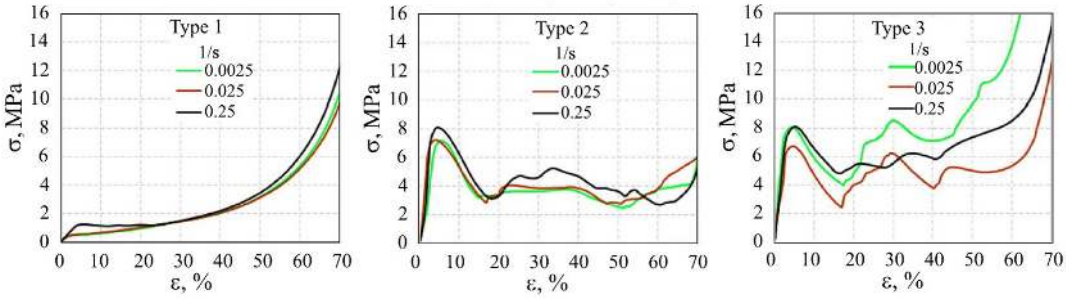

Figure 3: Stress-strain curves of unreinforced (type 1), transverse reinforced (type 2), and longitudinal reinforced (type 3) foam samples for different strain rates.

As it can be seen from the Figure 3 above that the resulting stress-strain curves exhibit the same three distinct regions regardless of the position of the reinforcement used and the strain rate applied. Namely, there is a narrow linear elastic region, followed by long yielding (during which the critical mechanisms of fracture emerge) and by densification with a sharp increase in stress σ at almost constant deformation ε. The stress-strain curve of unreinforced samples shows a smooth transition from the linear elastic region to the yield region and to the densification region. A higher strain rate led to an extension in the linear elastic region and an almost straight line in the plateau region without a significant change in stress. This was due to the progressive and controlled deformation of the cell walls in the foam [27]. In contrast, the stress-strain curves of transverse and longitudinal reinforced samples show a peak in yield stress at the end of the elastic region. In addition to that, the longitudinal reinforced samples exhibit stress fluctuations in the yield region and an abrupt transition to the densification region. The fluctuations can be related to folds that appear on the sides of reinforced samples during loading. They (fluctuations) are seen between yield point and compressive deformation.

At all strain rates, the stress-strain curve exhibited a yield point with an initial peak stress (y) value at the end of linear elastic region. Figure 3 shows that reinforced samples exhibit a sharp drop in yield stress after its peak was attained. At the same time, the transverse reinforced foams showed a larger stress drop than those reinforced longitudinally. The largest difference in stress (≈56% for transverse reinforced samples and ≈62% for longitudinal reinforced samples) was obtained at the strain rate of 0.025 s^{-1}. An increase in the strain rate resulted in slightly smaller stress drops (≈37%), but this was only the case for transverse reinforced samples. The unreinforced foams did not show such a decrease in stress at either of the strain rates.

The strain rate is an important factor influencing the energy absorption behavior of the composite foam. Figure 4 shows the specific absorption energies depending on the strain rate applied.

The energy absorption increased almost linearly with increasing strain rate until densification. For the unreinforced samples, an increase in the strain rate was accompanied by a dramatic increase in W (almost 1.5 times) at the cross-section with the densification region. This phenomenon is due to the collapse in the microstructure and friction between the cell walls during the compression test [28]. The linear relationship between energy absorption and strain rate in the reinforced samples was observed before the densification point. The energy absorption capacity of the transverse reinforced foams increased by approximately 1 MJ/m^3 at a strain rate to 0.025 s^{-1}. Further increase in the strain rate led to minor changes in the W-ε dynamics. In contrast, the longitudinal reinforced foams demonstrated the greatest energy absorption capacity at the lowest strain rate (0.0025 s^{-1}). A higher strain rate led to a decrease in energy absorption and with the highest strain rate applied (0.25 s^{-1}) the energy absorption became higher by almost 2 MJ/m^3. This enhancement was due to the variation in the deformation mechanisms.

The deformation sequences for the studied composites are depicted in Figure 5. As it can be seen, the deformation mechanisms tend to vary depending on the reinforcement used. The conventional $AlSi_{10}Mg$ alloy (unreinforced sample), for example, deforms in a controlled manner, whereas the reinforced specimens tend to crack on the sides as the loading increases, which happens because of the appearance of folds. The center of the reinforced composites did not deform due to a strong bond between the matrix and reinforcement. The movement of the reinforcing mesh was conditioned by the movement of the parts of foam with respect to the rest of the foam. In addition to that, the sample could be displaced from the loading axis as a result of poor contact between the sample and the details of the installation. However, this problem can be solved by proper geometry of the samples and local deformation of foam.

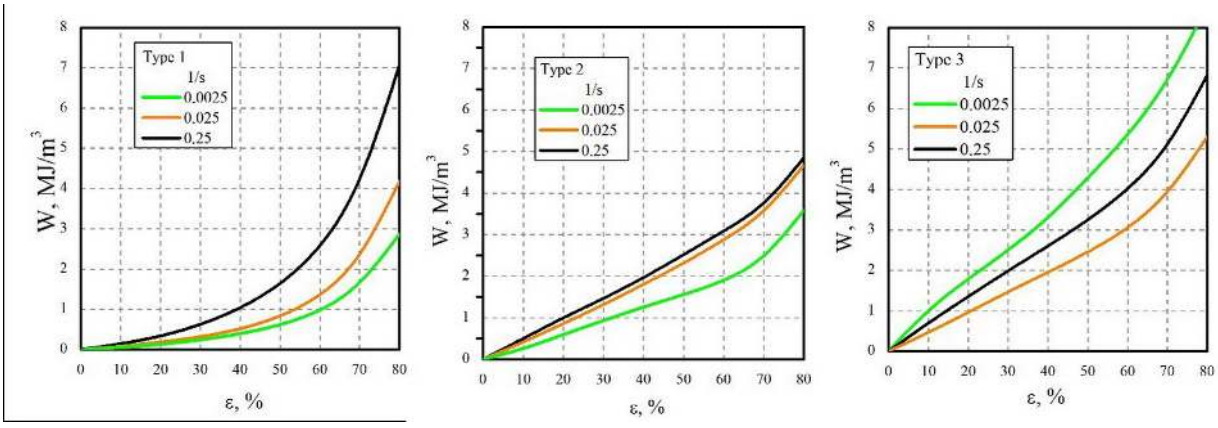

Figure 4: Specific energy absorption-strain curves of unreinforced (type 1), transverse reinforced (type 2), and longitudinal reinforced (type 3) foam samples for different strain rates.

4 Discussion

The experiments reveal that the yield region of both (transverse and longitudinal) reinforced foams shows a pronounced serrated character after σ_y, while none stress fluctuations in the case of unreinforced samples were found. The absence of stress fluctuations in unreinforced samples may be related to continuous hardening of these samples on the yield region. The serrated character of stress-strain curves for reinforced foams is largely due to the plastic deformation of the reinforcement, as well as the brittleness of aluminum alloys used for the production of foam [29, 30]. Due to the orientation of the reinforcements, significant variation in stress can be observed, specifically the longitudinal reinforced foams exhibit a pronounced character of the jump-like dynamics. This is due to the higher values of plastic deformation for longitudinal reinforcements (α = 90 °) than transverse reinforcements ((α = 0) [31].

Figure 6 depicts the main mechanical properties variation of the investigated foams with different strains. As can be seen, the investigated mechanical properties tend to vary depending on the reinforcement. Foams without reinforcements were found to present a 7 times lower quasi-elastic modulus on the linear elastic region than those with reinforcements (Figure 6a), although the weight of the material was only 7-10% lower due to the absence of the mesh. As the strain rate increases, the E_{qe} values of foams without reinforcements and with transverse reinforcements tend to go up by 23% and 20%, respectively. With longitudinal reinforcements, however, the E_{qe} values fell by 16%. Such a behavior suggests that the reinforced samples have higher elastic properties, even though the weight of these samples does not change much due to the high elasticity of the steel mesh used [32].

The strength properties (σ_y and σ_{pl}) follow a similar pattern. The yield point values σ_y of reinforced foams were 4 times higher than unreinforced ones (Figure 6b). The presence of transverse and longitudinal reinforcements increased the plateau stress by 2 and 4 times (Figure 6c), respectively, which indicates an enhancement of strength properties. However, the differences were observed with increasing strain rates. Foams without reinforcements and with transverse reinforcements show a linear association, while the presence of longitudinal reinforcement leads to a 16-19% decrease in σ_y and σ_{pl} at a strain rate of 0.025 s^{-1}, followed by a return to initial values with increasing strain rate. Conclusively, the reinforcement is a contributing factor in strength performance of $AlSi_{10}Mg$ foams. In addition, the compressive strength of reinforced composite foams strongly depends on the orientation of the reinforcement and is always higher when the foam is reinforced in longitudinal direction ((α = 90 °C). The expanded sheets are stronger in longitudinal direction because of larger load-bearing section (Figure 1).

Reinforced foams also demonstrate higher values of compressive strength and energy absorption (Figure 6d-f). The compressive strength σ_D of foams with longitudinal reinforcements was 2 times the compressive strength of foams with transverse reinforcements, while the unreinforced samples demonstrated higher compressive strength performances at lower (0.0025 s^{-1}) strain rates (Figure 6d). However, these values were observed at different densification strains ε_D: at 39% for unreinforced foams, at 68% for transverse reinforced foams, and at 47% for longitudinal reinforced foams (Figure 6e). The relatively high densification strains of reinforced samples at low strain rates can be related to the cellular structure of the mesh, which compensates for the brittle deformation behavior of the foamed material. The absence of reinforcement increased the den-

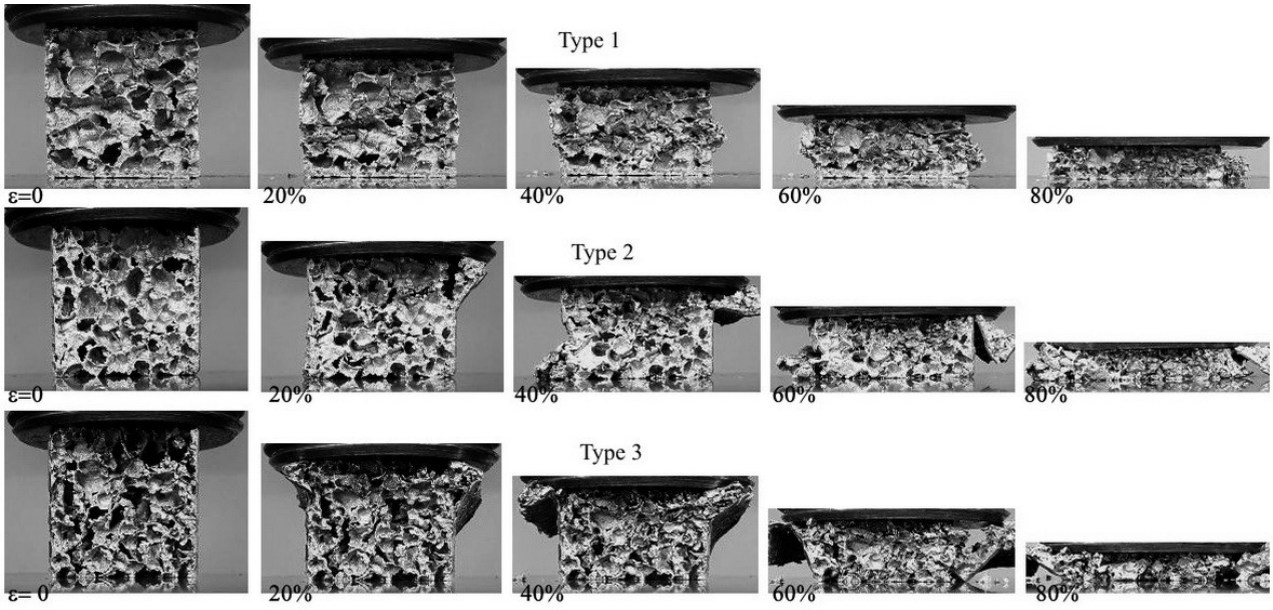

Figure 5: Images illustrating the deformation behavior of unreinforced (type 1), transverse reinforced (type 2), and longitudinal reinforced (type 3) foam samples at 0.025 s^{-1} strain rate.

sification strain up to 33% strain with increasing strain rate (Figure 6e). Contrariwise, an increase in the strain rate lead to a 36% linear increase in densification stress σ_D with transverse reinforcement, accompanied by a non-linear variation of ε_D values. With the presence of longitudinal reinforcement, the association between densification stress and strain is also nonlinear, as evidenced by a 36% drop in σ_D following a change in the strain rate by one order of magnitude, while a further increase in the strain rate came with a 30% densification stress drop. In cases with the absence of reinforcement, the strain rate increase by one order of magnitude enhanced the densification stress up to 61%, while a further increase in the strain rate reduced it to 54%. This behavior was due to the softening of the cell walls, while the presence of reinforcement increased the σ_D values at higher strains because of the high strength properties of the cellular mesh. These results are consistent with previous research [33], where the strength properties of composite foams were closely related to the orientation of the reinforcement and on the shape of the samples. The present work shows that longitudinal reinforcements lead to higher strength and densification properties, but the enhancement can only be reached if the reinforcing mesh is rolled into a cylinder.

Figure 6f shows how the specific energy absorption at densification strain of the investigated samples changes with increasing strain rate. As can be seen, the relationships are almost linear. The energy absorption properties of reinforced foams are much higher when compared to unreinforced samples (i.e., 4.5 times with longitudinal reinforcement and 3.7 times with transverse reinforcement). However, an increase in the strain rate led to a decrease in W_D values of reinforced foams (i.e., 33% and 37% from the initial value). In contrast, the unreinforced samples demonstrated a linear increase (39%) in W_D values with increasing strain rate. Both strength and energy absorption reduction properties show the same trend with the presence of reinforcement. A lower reduction in W_D values of transverse reinforced foams is associated with a more stable deformation mechanism when compared to foams with longitudinal reinforcements. This feature can be easily seen from Figure 2, where the stress-strain curves show much lower oscillation amplitudes for all investigated strain rates with the presence of transverse reinforcement, especially the yield region. The smallest difference between the energy absorption properties of unreinforced and reinforced foams is observed at high strain rates (Figure 6f). The greatest difference in stress values was observed at low strain rates. In addition, there were more differences with respect to strength properties reduction with increasing strain rate in the case of reinforced foams than in the case of unreinforced. These differences stem from the following effects: the mechanical properties of the foam matrix material, the mechanism of foam deformation, and the mechanical properties of the reinforcement. Due to the emergence of dynamic recrystallization and softening of the matrix material at low strain, the deformation behavior of the foams changed along with a significant reduction in mechanical properties [34]. As the

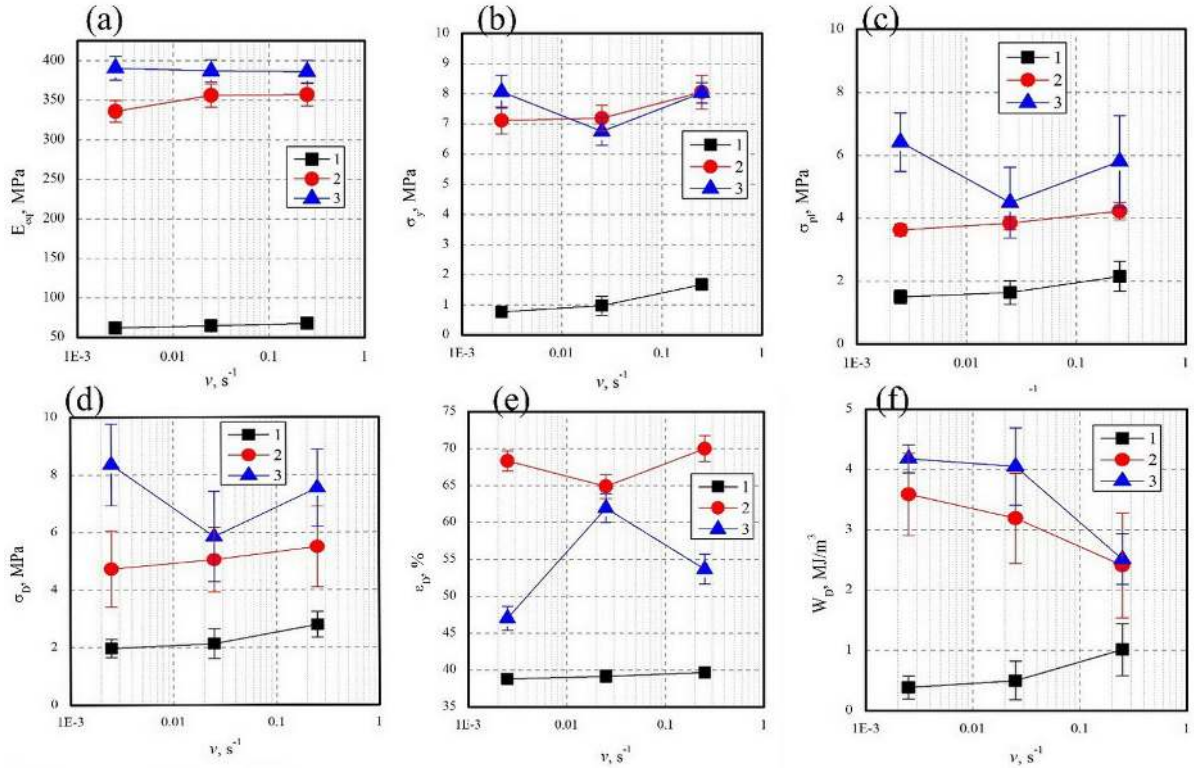

Figure 6: The mechanical properties (E_{qe}, σ_y, σ_{pl}, σ_D, ε_D, W_D) of unreinforced (type 1), transverse reinforced (type 2), and longitudinal reinforced (type 3) foam samples for different strain rates.

strain rate increased, the foam exhibited a brittle deformation mechanism followed by plastic behavior with plastic-to-brittle transition. The reinforcements were found to take up most of the deformation mechanisms, influencing both an increase and reduction of the mechanical properties. Hence, the positioning of reinforcement in the composite matrix is also a dominant deformation mechanism besides foam porosity and foam density.

Further research may involve replacing steel sheets with more complex three-dimensional reinforcements. The results of this work can be employed in numerical calculations to determine the proper structural parameters of the reinforcing mesh to obtain products with high impact resistance and minimum weight. Further works can focus on varying temperatures at different strain rates. The obtained findings can be applied in modeling various metal structures to reinforce foams. The calculated basic mechanical characteristics depending on the load rate at different orientations of the reinforcing mesh can be used in software applications to analyze the impact resistance of various structures made of reinforced composite foams.

5 Conclusions

This work was concerned with the quasi-static compressive mechanical properties of closed-cell aluminum alloy foams reinforced with a steel mesh with different call orientations at different strain rates. The investigated mechanical properties (i.e, the quasi-elastic modulus, yield stress, plateau stress, densification stress, densification strain, and the specific energy absorption at densification strain) were obtained from the experimental stress-strain curves. The results show that the deformation behavior and mechanical properties of reinforced foams strongly depend on the positioning of the reinforcement according to the loading direction. The reinforcements were found to affect the magnitude of the compressive plateau stress. The foam samples with longitudinal reinforcement exhibited a high energy absorption capacity thanks to the high compressive strength. The strength properties and energy absorption capacity of unreinforced foam sample improved linearly with increasing strain rate because of dynamic recrystallization and softening of the foam matrix material. The deformation behavior of reinforced foam samples was a function of the cell orientation. It was found that the mechanical properties reduction of transverse reinforced foams was slightly lower

compared to foams with longitudinal reinforcement at varying strain rates. The reinforcements took up most of the deformation mechanisms, resulting in a nonlinear behavior of mechanical properties. The results of the experiments can be employed to modelling and obtain impact-resistant fillers for complex structures in transport construction.

Funding information: The authors state no funding involved.

Author contributions: All authors have accepted responsibility for the entire content of this manuscript and approved its submission.

Conflict of interest: The authors state no conflict of interest.

Data availability statement: The datasets generated during and/or analysed during the current study are available from the corresponding author on reasonable request.

References

[1] Bahl S. Fiber reinforced metal matrix composites-a review. Mater Today Proc. 2021;39:317-23.
[2] Imran M, Khan AA. Characterization of Al-7075 metal matrix composites: a review. J Mater Res Technol. 2019;8(3):3347-56.
[3] Reddy AP, Krishna PV, Rao RN, Murthy NV. Silicon carbide reinforced aluminium metal matrix nano composites-a review. Mater Today Proc. 2017;4(2):3959-71.
[4] Nicholls CJ, Boswell B, Davies IJ, Islam MN. Review of machining metal matrix composites. Int J Adv Manuf Technol. 2017;90(9-12):2429-41.
[5] Jawalkar CS, Verma AS, Suri NM. Fabrication of aluminium metal matrix composites with particulate reinforcement: a review. Mater Today Proc. 2017;4(2):2927-36.
[6] Li ZH, Nie YF, Liu B, Kuai ZZ, Zhao M, Liu F. Mechanical properties of AlSi10Mg lattice structures fabricated by selective laser melting. Mater Des. 2020;192:108709.
[7] Binesh F, Zamani J, Ghiasvand M. Ordered structure composite metal foams produced by casting. Int J Met. 2018;12(1):89-96.
[8] Rathod BS, Pandey B. Effect of turning parameters on aluminium metal matrix composites-a review. In: IOP Conference Series: Materials Science and Engineering (Vol. 225, No. 1). IOP Publishing; 2017. p. 012276.
[9] Amaro AM, Neto MA, Cirne JS, Reis PN. Mechanical characterization of different aluminium foams at high strain rates. Materials. 2019;12(9):1428.
[10] Su M, Wang H, Hao H. Compressive properties of aluminum matrix syntactic foams prepared by stir casting method. Adv Eng Mater. 2019;21(8):1900183.
[11] Kırmızı G, Arık H, Çinici H. Experimental study on mechanical and ballistic behaviours of silicon carbide reinforced functionally graded aluminum foam composites. Compos B Eng. 2019;164:345-57.
[12] Soltani N, Bahrami A, Pech-Canul MI. The effect of Ti on mechanical properties of extruded in-situ Al-15 pct Mg 2 Si composite. Metall Mater Trans A. 2013;44(9):4366-73.
[13] Rousta Z, Khosravi H, Tohidlou E. Effect of Er addition on the microstructural characteristics and compressive behavior of insitu Al-15 wt.% Mg2Si composites. J Sci Technol Compos. 2019;6(2):242-7.
[14] Huang Z, Zhang X, Yang C. Experimental and numerical studies on the bending collapse of multi-cell Aluminum/CFRP hybrid tubes. Compos B Eng. 2020;181:107527.
[15] Kaczyński P, Karliński J, Hawryluk M. Experimental and numerical studies of the behavior and energy absorption of foam-filled circular tubes. Arch Metall Mater. 2020;65(2):521-7.
[16] Formisano A, Barone A, Carrino L, De Fazio D, Langella A, Viscusi A, et al. Improvement of the mechanical properties of reinforced aluminum foam samples. In: AIP Conference Proceedings (Vol. 1960, No. 1). AIP Publishing LLC; 2018. p. 100007.
[17] Viscusi A, Carrino L, Durante M, Formisano A. On the bending behaviour and the failure mechanisms of grid-reinforced aluminium foam cylinders by using an experimental/numerical approach. Int J Adv Manuf Technol. 2020;106(5):1683-93.
[18] Szwedowicz D, Estrada Q, Cortes C, Bedolla J, Alvarez G, Castro F. Evaluation of energy absorption performance of steel square profiles with circular discontinuities. Lat Am J Solids Struct. 2014;11(10):1744-60.
[19] Zahran MS, Xue P, Esa MS, Abdelwahab MM, Lu G. A new configuration of circular stepped tubes reinforced with external stiffeners to improve energy absorption characteristics under axial impact. Lat Am J Solids Struct. 2017;14(2):292-311.
[20] Solórzano E, Rodríguez-Perez MA, Reglero JA, de Saja JA. Mechanical behaviour of internal reinforced aluminium foams. Adv Eng Mater. 2007;9(11):955-8.
[21] Jerz J, Mináriková N, Marsavina L, Linul E. Scaling of compression strength in disordered solids: Metallic foams. Frattura Integr Strutt. 2016;10(36):55-62.
[22] Uzun A. Production of aluminium foams reinforced with silicon carbide and carbon nanotubes prepared by powder metallurgy method. Compos B Eng. 2019;172:206-17.
[23] Acerinox. Stainless Steel Grade; 2020. [cited 2021 April 22] Available from: https://www. acerinox.com/en/productos/stainless-steel-grade/EN-1.4301 –AISI-304-00001/
[24] Santosa SP, Wierzbicki T, Hanssen AG, Langseth M. Experimental and numerical studies of foam-filled sections. Int J Impact Eng. 2000;24(5):509-34.
[25] ISO 13314:2011. Mechanical testing of metals – Ductility testing – Compression test for porous and cellular metals; 2011 [cited 2021 April 22] Available from: https://www.iso.org/standard/53669.html
[26] Movahedi N, Murch GE, Belova IV, Fiedler T. Manufacturing and compressive properties of tube-filled metal syntactic foams. J Alloys Compd. 2020;822:153465.
[27] Hangai Y, Saito K, Utsunomiya T, Kuwazuru O, Yoshikawa N. Fabrication and compression properties of functionally graded foam with uniform pore structures consisting of dissimilar A1050 and A6061 aluminum alloys. Mater Sci Eng A. 2014;613:163-70.
[28] Sauter T, Kratz K, Lendlein A. Pore-size distribution controls shape-memory properties on the macro-and microscale of polymeric foams. Macromol Chem Phys. 2013;214(11):1184-8.

[29] Yang D, Wang H, Guo S, Chen J, Xu Y, Lei D, et al. Coupling effect of porosity and cell size on the deformation behavior of Al alloy foam under quasi-static compression. Materials. 2019;12(6):951.
[30] Atturan UA, Nandam SH, Murty BS, Sankaran S. Deformation behaviour of in-situ TiB2 reinforced A357 aluminium alloy composite foams under compressive and impact loading. Mater Sci Eng A. 2017;684:178-85.
[31] Huang H, Wang J, Liu W. Mechanical properties and reinforced mechanism of the stainless steel wire mesh–reinforced Al-matrix composite plate fabricated by twin-roll casting. Adv Mech Eng. 2017;9(6):1687814017716639.
[32] Yang X, Yu J, Xiao T, Hu Z, He YL. Design and operating evaluation of a finned shell-and-tube thermal energy storage unit filled with metal foam. Appl Energy. 2020;261:114385.
[33] Bunjan I, Grilec K, Ćorić D. Investigation and statistical evaluation of reinforced aluminum foams. Processes. 2021;9(2):315.
[34] Hu X, Gong X. Pore-scale numerical simulation of the thermal performance for phase change material embedded in metal foam with cubic periodic cell structure. Appl Therm Eng. 2019;151:231-9.